Stereoisomerism of Molecular Multipropellers. 2. Dynamic Stereochemistry of Bis- and Tris-Triaryl Systems

Josep Sedó,[†] Nora Ventosa,[†] Mª Antònia Molins,[‡,§] Miquel Pons,*[,‡] Concepció Rovira,[†] and Jaume Veciana*[,†]

Institut de Ciència de Materials de Barcelona (CSIC), Campus Universitari de Bellaterra, 08193 Cerdanyola, Spain, and Departament de Química Orgànica and Serveis Científico-Tècnics de la Universitat de Barcelona, C/Martí Franquès, 1-11, 08028-Barcelona, Spain

vecianaj@icmab.es

Received March 29, 2000 (Revised Manuscript Received November 8, 2000)

The dynamic stereochemistry of bis- and tris-triaryl systems, the most simple "molecular multipropellers", is discussed on the basis of an extension of a systematic stereochemical analysis based on a symmetry-adapted symbolic notation developed specifically for these molecules. A suitable theoretical basis for our study is provided by the classical hypotheses concerning the dynamics of simple triaryl systems as formulated by Mislow and co-workers (*J. Am. Chem. Soc.* **1973**, *95*, 1535−1547), which, once applied to molecular multipropellers, show the existence of two modes of rearrangement for each propeller. Interconversion graphs for all molecules under study, covering a wide span of structural complexity, are presented. A complete NMR study of a two- and a three-propeller molecule indicates that all experimentally observable exchange pathways are indeed predicted by theoretical analysis. Moreover, quantitative analysis of 2D-EXSY experiments affords the activation energy of the subset of pathways that give rise to observable interconversions on the NMR time scale. Assuming that two-ring flips are the threshold mechanism for individual propeller interconversion, the experimental evidence indicates a preference for the flip of the central ring and one of the outer rings over the flip of two outer rings.

Introduction

The dynamics of interconversion processes in systems presenting restricted conformational equilibria, such as triarylmethanes and many other structurally related molecules, generically called "molecular propellers", attracted much attention in the mid-1970s, as they played a fundamental role in the development of key concepts in stereochemistry.[1,2] Although several of these and other similar systems have been thoroughly investigated as far as their static and dynamic stereochemistry is concerned,[3] very little systematic work has been published concerning molecules having more than one propeller-like moiety in their structures.[3j,4,5] All these studies have led to the development of a solid theoretical framework based on group theory that permits the investigation of the number and symmetry of conformational isomers and the analysis of their interconversion paths.[2,6]

The purpose of this contribution is to apply the basic principles governing the dynamic stereochemistry of single propellers, already developed in the seminal work of Mislow and co-workers[1−3,6] to extended systems having more than one propeller-like moiety in their structures; for which we coined the generic name "molecular multipropellers".[7] In this respect, the present paper, which discusses the dynamic stereochemistry of molecules belonging to families **1** and **2**, is aimed to providing both a theoretical framework and suitable experimental evidence for the preferred conformational dynamics of multipropeller systems.

Compounds **1** and **2** are constituted by two and three overlapping polychlorinated triphenylmethane or tri-

* To whom correspondence should be addressed. E-mail: mpons@qo.ub.es.
[†] Institut de Ciència de Materials de Barcelona, CSIC.
[‡] Departament Química Orgànica, Universitat de Barcelona.
[§] Serveis Científico-Tècnics, Universitat de Barcelona.

(1) Gust, D.; Mislow, K. *J. Am. Chem. Soc.* **1973**, *95*, 1535−1547.
(2) Mislow, K. *Acc. Chem. Res.* **1976**, *9*, 26−33.

(3) Among others these comprise studies with the following. (a) Di- and triarylboranes, see: Blount, J. F.; Finocchiaro, P.; Gust, D.; Mislow, K. *J. Am. Chem. Soc.* **1973**, *95*, 7029−7037. Blount, J. F.; Finocchiaro, P.; Gust, D.; Mislow, K. *J. Am. Chem. Soc.* **1973**, *95*, 7019−7028. (b) Trialkoxylmethanes, see: Willem, R.; Hoogzand, C. *Org. Magn. Reson.* **1979**, *12*, 55−58. (c) Triarylamines, see: Glaser, R.; Blount, J. F.; Mislow, K. *J. Am. Chem. Soc.* **1980**, *102*, 2777−2786. (d) Tetraarylcyclopentadienones, see: Willem, R.; Pepermans, H.; Hoogzand, C.; Hallenga, K.; Gielen, M.; *J. Am. Chem. Soc.* **1981**, *103*, 2297−2306. Willem, R.; Jans, A.; Hoogzand, C.; Hoogzand, C.; Gielen, M.; Binst, G. V.; Pepermans, H. *J. Am. Chem. Soc.* **1985**, *107*, 28−32. (e) Tetraarylethanes and tetraarylethylenes, see: Willem, R.; Pepermans, H.; Hallenga, K.; Gielen, M.; Dams, R. *J. Org. Chem.* **1983**, *48*, 1890−1898. (f) Hexaalkylbenzenes, see: Weissensteiner, W.; Gutierrez, A.; Radcliffe, M. D.; Siegel, J.; Singh, M. D.; Tuohey, P. J.; Mislow, K. *J. Org. Chem.* **1985**, *50*, 5822−5827. Siegel, J.; Gutierrez, A.; Schweizer, W. B.; Ermer, O.; Mislow, K. *J. Am. Chem. Soc.* **1986**, *108*, 1569−1575. (g) Hexaarylbenzenes and related compounds, see: Gust, D. *J. Am. Chem. Soc.* **1977**, *99*, 6980−6982. Gust, D.; Patton, A. *J. Am. Chem. Soc.* **1978**, *100*, 8175−8181. Gust, D.; Fagan, M. W. *J. Org. Chem.* **1980**, *45*, 2511−2512. Pepermans, H.; Willem, R.; Gielen, M.; Hoogzand, C. *J. Org. Chem.* **1986**, *51*, 301−306. (h) Hexaalkoxylbenzenes, see: Singh, M. D.; Siegel, J.; Biali, S. E.; Mislow, K. *J. Am. Chem. Soc.* **1987**, *109*, 3397−3402. (i) Decaalkylbiphenyls, see: Biali, S. E.; Kahr, B.; Okamoto, Y.; Aburatani, R.; Mislow, K. *J. Am. Chem. Soc.* **1988**, *110*, 1917−1922. Biali, S. E.; Buda, A. B. *J. Org. Chem.* **1988**, *53*, 135−139. Marks, V.; Gottlieb, H. E.; Biali, S. E. *J. Am. Chem. Soc.* **1997**, *119*, 9672−9679. (j) Molecules with more than one propeller subunit, see: Linder, A. B.; Grynszpan, F.; Biali, S. E. *J. Org. Chem.* **1993**, *58*, 6662−6270. Selzer, T.; Rappoport, Z. *J. Org. Chem.* **1996**, *61*, 7326−7334.

(4) Veciana, J.; Rovira, C.; Crespo, M.-I.; Armet, O.; Domingo, V. M.; Palacio, F. *J. Am. Chem. Soc.* **1991**, *113*, 2552−2561.

(5) Veciana, J.; Rovira, C.; Ventosa, N.; Crespo, M.-I.; Palacio, F. *J. Am. Chem. Soc.* **1993**, *115*, 57−64.

10.1021/jo000474g CCC: $20.00 © 2001 American Chemical Society
Published on Web 02/06/2001

Scheme 1

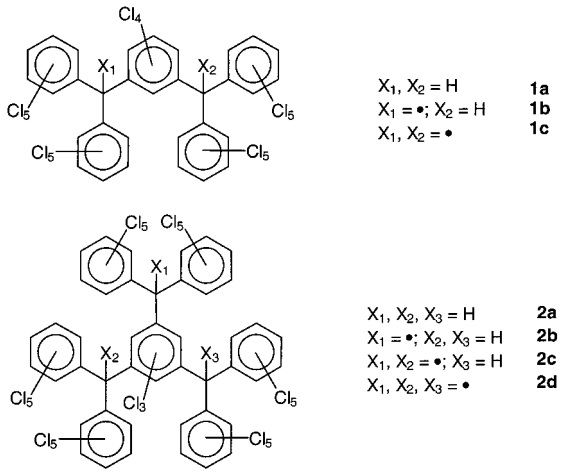

phenylmethyl moieties, respectively. Each triaryl moiety of **1** and **2** is forced by the bulky chlorine atoms that substitute all the aromatic ortho positions, crowding the surroundings of the carbon atoms central to each moiety and subsequently forcing the noncoplanarity of adjacent rings. Consequently, each triaryl moiety of **1** and **2** adopts a propeller-like arrangement and they can be taken as model structures for what may be generically called "molecular multipropellers". Compounds **1** and **2** have a superficial resemblance to substituted hexaarylbenzenes, studied by Gust et al.,[3g] because of the presence of six aromatic rings around the central benzene. The complex stereoisomerism and stereoisomerization behavior of substituted hexaarylbenzenes were elegantly analyzed by these authors using group-theoretical methods where isomers are treated in terms of permutations of ligands in sites on a rigid skeleton of a given symmetry.[3g] However, the analysis of stereoisomerism of compounds **1** and **2** using the same theoretical methodology becomes extremely cumbersome because they are much more stereochemically complex due to their lower symmetries and therefore may potentially display some very subtle isomerization phenomena.

Results and Discussion

Modes of Rearrangement in Molecular Multipropellers. Propeller-like structures, such as those adopted by di- and triaryl systems,[8] can undergo isomerization by rotation of aromatic rings involving either the transient passage of the ring across the propeller plane—defined by the three *ipso*-carbon atoms—or through a direction perpendicular to this plane. The latter movement is known as a *ring flip*.[1] Both theoretical[9] and experimental studies[1−3,10−12] have shown that propeller-like systems undergo conformational changes exclusively through *simultaneous* or *correlated* rotations of all their aromatic rings, thus limiting the number of possible interconversion pathways. For a three-bladed propeller only $2^3 = 8$ pathways are possible. These can be classified according to the number of ring flips involved. The remaining aromatic rings rotate across the propeller plane. There are three *one-ring flip* and *two-ring flip* pathways, but only one *zero-ring flip* and one *three-ring flip* pathway (Figure 1).[1,13] Although one example of one-ring flip threshold mechanism has been reported to date,[14] two-ring flip pathways seem to be the threshold mechanism for many known propeller-like systems.[1−3,9,10] It is worth mentioning that all eight interconversion pathways led to a change in helicity, and in the absence of local C_2 symmetry, each different pathway led to a distinct, nonsuperposable structure.

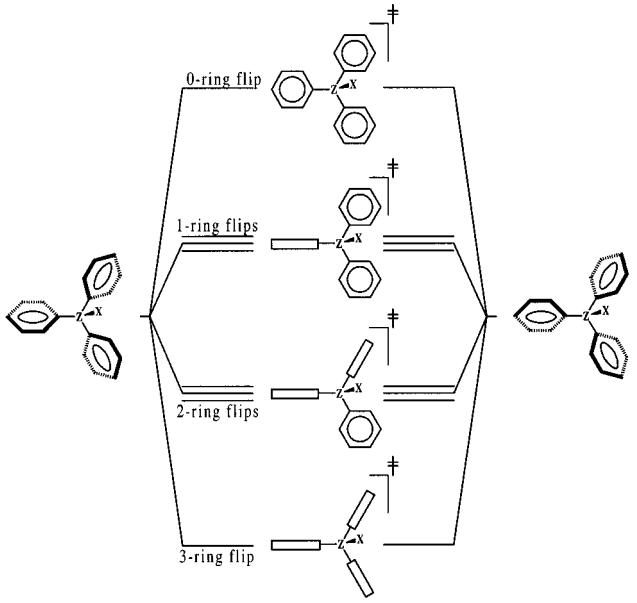

Figure 1. Transition states corresponding to the four predicted types of interconversion mechanisms for single three-bladed propellers.

In multipropeller systems, the same principles apply for each propeller. We assume that conformational changes in two different propellers within the same molecule are very unlikely to occur simultaneously as the interconversion barriers would be twice the value observed for single propellers which is already very high: over 20 kcal·mol^{-1} when bulky ortho substituents are present.[1−3,10,15] Thus, we can analyze the stereochemical consequences of the different mechanisms independently for each triaryl moiety of a given multipropeller. In each case, the moieties not undergoing conformational changes are considered subsidiary and schematized as pendant groups, A and B, located in the meta positions of one of the aromatic groups experiencing the conformational change.

(6) (a) Hässelbarth, W.; Ruch, E. *Theor. Chim. Acta* **1973**, *29*, 259−268. (b) Brocas, J.; Gilen M.; Willem, R. *The Permutational Approach to Dynamic Stereochemistry*; McGraw-Hill: New York, 1983.

(7) Sedó, J.; Ventosa, N.; Molins, M. A.; Pons, M.; Rovira, C.; Veciana, J. *J. Org. Chem.* **2001**, *66*, 1567−1578.

(8) The terms *di-* and *triaryl systems* used throughout describe molecules containing moieties such as Ar^1Ar^2ZXY (or Ar^1Ar^2ZY) and $Ar^1Ar^2Ar^3ZX$ (or $Ar^1Ar^2Ar^3Z$), respectively, where Z is the central atom of the referred moiety, having either sp^2 (Z) or sp^3 (ZX) hybridization.

(9) Andose, J. D.; Mislow, K. *J. Am. Chem. Soc.* **1974**, *96*, 2168−2176.

(10) Finocchiaro, P.; Gust, D.; Mislow, K. *J. Am. Chem. Soc.* **1974**, *96*, 3198−3205; **1974**, *96*, 3205−3213.

(11) Willem, R.; Hoogzand, C. *Org. Magn. Reson.* **1979**, *12*, 55−58.

(12) Sabacky, M. J.; Johnson, S. M.; Martin, J. C.; Paul, I. C. *J. Am. Chem. Soc.* **1969**, *91*, 7542.

(13) Kurland, R. J.; Schuster, I. I.; Colter, A. K. *J. Am. Chem. Soc.* **1965**, *87*, 2279.

(14) Ito, S.; Fujita, M.; Asao, T. *Bull. Chem. Soc. Jpn.* **1995**, *68*, 3611−3620.

(15) (a) Crespo, M.-I. Ph.D. Thesis, Institut Quìmic de Sarriá (Universitat Ramón Llull), Barcelona, 1991; p 306. (b) Ventosa, N. Ph.D. Thesis, Institut Quìmic de Sarriá (Universitat Ramón Llull), Barcelona, 1996; p 393.

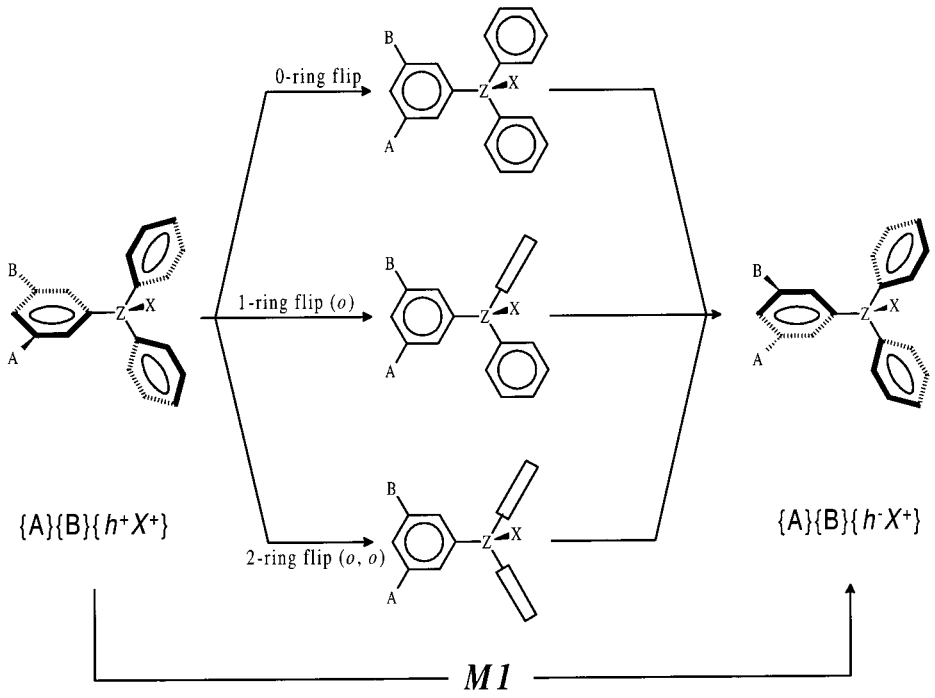

Figure 2. Set of interconversion mechanisms belonging to the mode of rearrangement M_1.

Looking at the structures of molecules **1** and **2**, it is clear that only the outer rings have C_2 symmetry. Substituents A and B in the inner rings are, in general, nonequivalent, and these rings are therefore not C_2 symmetric. More specifically, for molecules pertaining to series **1**, A and B are always constitutionally different. In series **2**, A and B are constitutionally equivalent in **2a** and **2d** but differ from a stereochemical point of view as each moiety supports one or two stereogenic elements with potentially different configurations.

Interconversion pathways operating in a three-bladed propeller structure with two nonequivalent pendant groups breaking the local C_2 symmetry of one of the rings can be grouped in two *modes of rearrangement* named as M_1 and M_2,[16] according to the relationship between the initial and final conformations they connect. M_1 modes involve the flip of rings with local C_2 symmetry (outer rings, "*o*") and result only in the reversal of the helicity of the triaryl moiety affected (Figure 2). M_2 mechanisms are associated with the flip of non-C_2 symmetric rings (inner rings, "*i*") and exchange the position of substituents A and B with respect to the ring rotation axis (Figure 3), a movement that is equivalent to changing the orientation of the X substituent, if present.[17] Structural changes associated to the two modes of rearrangement are summarized in Table 1. Table 2 shows the grouping of the interconversion pathways in the two modes of rearrangement. Note that ring flips involving the two equivalent outer rings are indistinguishable and the number of mechanisms is reduced from eight to six.

For a molecule with *n*-propellers, the maximum number of operationally distinguishable interconversion pathways is 2^n, although the actual number may be smaller because of degeneracy.

Symmetry-Adapted Symbolic Notation and Interconversion Graphs. In the preceding paper,[7] a specific, symmetry-adapted symbolic notation was developed and a set of "static" transformation rules, that enabled investigate the static stereochemistry of molecules **1a**−**c** and **2a**−**d** in a unified way, was derived.[7] We will show now that this symbolic notation is also appropriate for an accurate analysis of the conformational dynamics of these systems.

To determine all possible interconversion routes between the stereoisomers of molecules of series **1** or **2**, all operationally distinguishable interconversion pathways—4 and 6 for two- and three-propeller systems, respectively—are applied to each stereoisomer. The resulting static representations are analyzed and assigned to one of the real stereoisomers of the molecule by means of the "static" transformation rules.[18]

Theoretically predicted interconversion routes between different stereoisomers for each molecule may be suitably depicted by means of an interconversion graph. In order facilitate the interpretation, stereoisomers have been distributed in such a way that enantiomers are symmetry related in the graph. Specifically, for molecules of series **1**, a dashed line, denoted by σ, relates each stereoisomer from its corresponding enantiomer. Obviously, meso forms with C_s symmetry, when present, are placed over this enantiomerization line. With regard to the three-propeller molecules of series **2** we found that an inversion center, represented by an open dot denoted by an *e*, is a more suitable choice for relating enantiomers on the graph. Sets of paths connecting a given stereoisomer with its immediate neighbors will be hereafter called "*interconversion patterns*" and, as will be shown, they are extremely useful for the assignment of the stereoisomer.

(16) In our case, a *mode of rearrangement* is a set of elementary pathways, which are indistinguishable because they take place between the same initial and final stereoisomeric forms. For a more general definition, see ref 3e.

(17) The equivalence can be seen by rotating the resulting structure by 180° so that substituents A and B can be superimposed to those in the starting structure.

(18) See the preceding paper, ref 7, for the transformation rules of "static representations" and the procedure used for such analysis and assignment.

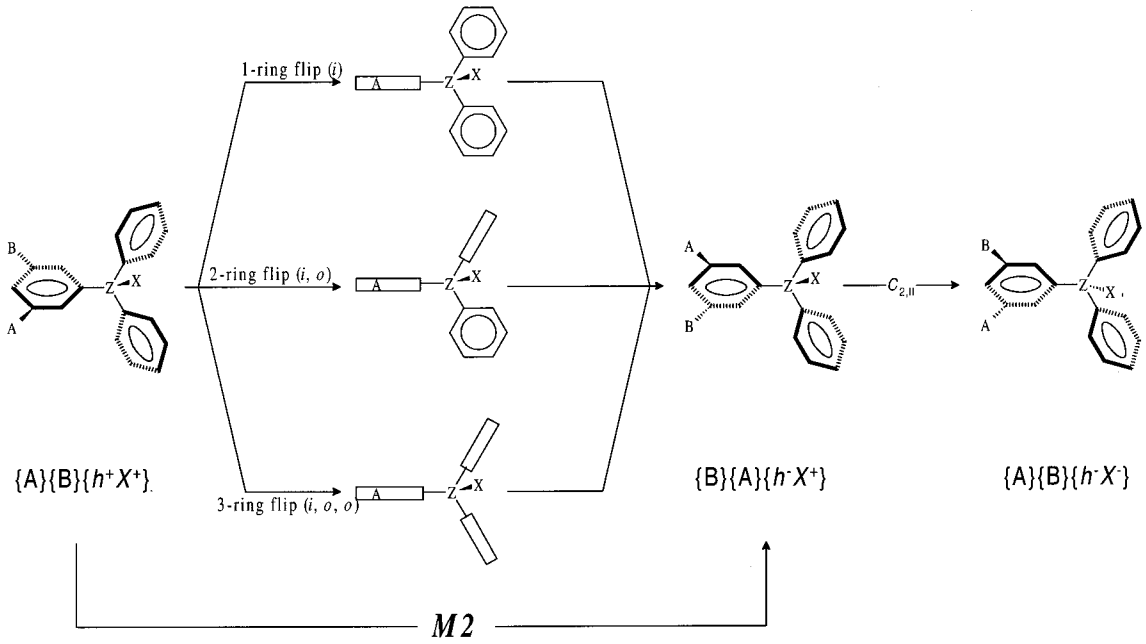

Figure 3. Set of interconversion mechanisms belonging to the mode of rearrangement M_2.

Table 1. Structural Changes Associated with the Two Modes of Arrangement for Multipropeller Systems 1 and 2

mode of rearrangement	helicity	orientation of central substituent	position of subsidiary triaryl moieties (A, B)
M_1	inversion	unchanged	unchanged
M_2	inversion	inversion	unchanged

Table 2. Mechanisms of Interconversion and Modes of Rearrangement for a Three-Bladed Propeller Generic Structure to Which Molecular Multipropellers 1 and 2 Conform

mechanism		mode of rearrangement
3-ring flip (o_1, o_2, i)	3-ring flip (o, o, i)	M_2
2-ring flip (o_1, o_2)	2-ring flip (o, o)	M_1
2-ring flip (o_1, i)	2-ring flip (o, i)	M_2
2-ring flip (o_2, i)		
1-ring flip (i)	1-ring flip (i)	M_2
1-ring flip (o_1)	1-ring flip (o)	M_1
1-ring flip (o_2)		
0-ring flip	0-ring flip	M_1

(a) Two-Propeller Molecular Systems. As shown in Figure 4 (top), the interconversion graph for **1c** is extremely simple and can be intuitively derived. For instance, it is easy to infer that, to convert a given chiral stereoisomer with C_2 symmetry—$\{h^+\}\{h^+\}$—into its enantiomer—$\{h^-\}\{h^-\}$—the passage through the meso form $-\{h^+\}\{h^-\}-$ is unavoidable provided that interconversions take place, as hypothesized, on one helix at a time. For C_2 stereoisomers, the 4-fold degeneracy of the interconversion mechanisms occurs—being thus maximal—since both helices are symmetry equivalent and non-X-substituted. As far as **1b** is concerned, the lack of symmetry in all stereoisomers explains the partial loss of degeneracy in the interconversion pathways and, consequently, the higher complexity of its interconversion graph (Figure 4, center). As a matter of fact, two distinct routes depart from the helix supporting two stereogenic elements whereas, due to the identity between M_1 and M_2, only one leaves the other moiety, showing that the helicity is the unique stereogenic element. Therefore, three distinct pathways leave each stereoisomer. Moreover, it should be noted that, despite the complete lack

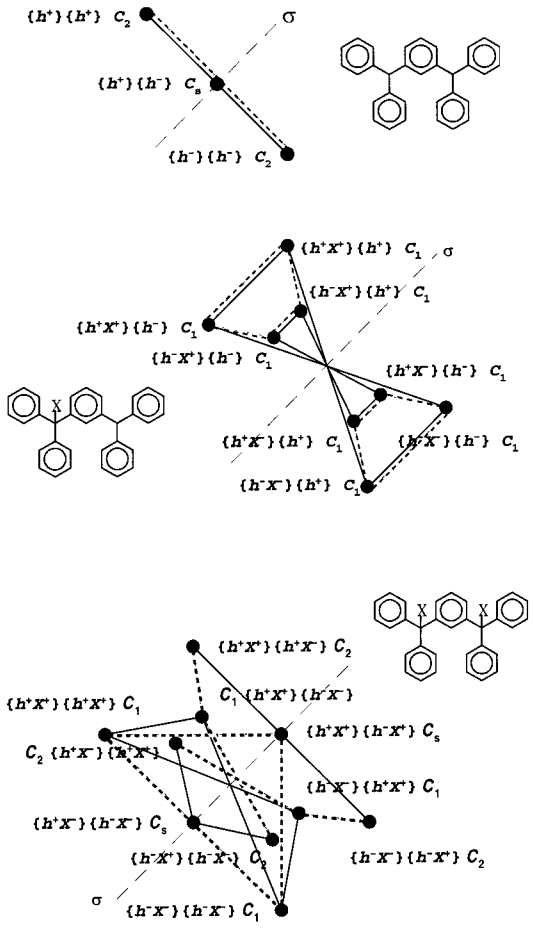

Figure 4. Interconversion graphs of molecules **1c** (top), **1b** (center), and **1a** (bottom). Short-dashed lines: M_1 pathways. Solid lines: M_2 pathways. Long-dashed lines (σ) denote mirror planes.

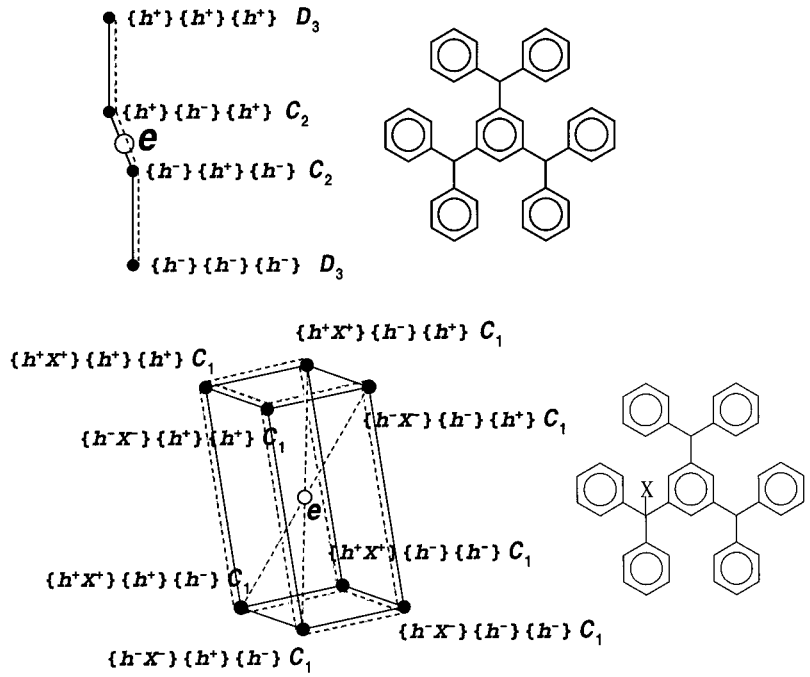

Figure 5. Interconversion graphs of molecules **2d** (top) and **2c** (bottom). Short-dashed lines: M_1 pathways. Solid lines: M_2 pathways. An open circle (*e*), central to each graph denotes an enantiomerization/inversion center.

of symmetry of the whole set of stereoisomers—all of them with C_1 symmetry—all the interconversion patterns of **1b** are identical. Finally, in proportion to its number of stereoisomers, molecule **1a** presents the most complex interconversion graph of all molecules pertaining to series **1** (Figure 4, bottom). Four distinct pathways leave each completely disymmetrical species (C_1), in accordance with the existence of four nonequivalent stereogenic elements in such species. In agreement with our expectations, this number is halved for C_2 stereoisomers because of symmetry degeneracy. As far as the meso (C_s) forms are concerned, the four routes would only be distinguishable in a chiral environment; i.e., in those surroundings in which enantiomers could be differentiated as well. On the other hand, achiral environments would make these pathways coincide in pairs, because both moieties, which are enantiotopic to each other, would then be indistinguishable. This situation may be easily viewed by "folding" the interconversion graph by the dashed line (σ).

(b) Three-Propeller Molecular Systems. The simplest three-propeller structure, exemplified by the triradical **2d**, has a characteristic linear interconversion graph (Figure 5, top), similar to that of **1a**. Thus, the stereoisomers with a high-symmetry content (D_3) occupy the ends of the graph, while the least symmetric ones (C_2) occupy the innermost positions. The 6-fold degeneracy shown by the interconversion paths of the D_3 stereoisomers of **2d** arises from all moieties having the same helicity, together with the existence of a single stereogenic element in each moiety.

The interpretation of the graph corresponding to the interconversions among the eight stereoisomers of biradical **2c** (Figure 5, bottom) is not so straightforward as that of **2d**, since not all degeneracies are obvious. As required, modes M_1 and M_2 have the same effect on moieties having helicity as the unique stereogenic element. With regard to the third moiety—the only one that supports an X substituent—M_1 and M_2 only coincide if the other two moieties are mutually homotopic. This may be easily justified by taking into account that if the subsidiary moieties are rotationally equivalent; the aromatic ring that supports them has C_2 symmetry and is thus invariant to binary in-plane rotations of the whole molecule. Clearly, thus, the chiral plane no longer exists. If, on the other hand, the subsidiary moieties are *not* rotationally equivalent—more specifically, when they present opposite helicities—the conformational modification affects changes in a chiral plane. Under these circumstances, two stereogenic elements come into play: if M_1 takes place, only the helicity is changed, otherwise (M_2), both the helicity and the configuration of the chiral plane are reversed.

At first sight, the monoradical **2b** presents the most complex interconversion graph (Figure 6), at least in view of the high number (20) of stereoisomers expected for this compound.[7] For clarity, those pertaining to the C_1 symmetry group have been placed on the vertexes of two octahedrons, while the rest (C_2) occupy positions in the graph external to the latter ones that define two rectangles. Compared with that of **2c**, this graph shows a smaller number of degenerate paths. Particularly, the single degeneracy in C_1 isomers arises from the equivalency of M_1 and M_2 on the only triaryl moiety without X substituent. As far as C_2 isomers are concerned, we should bear in mind that the two X-substituted moieties are related by the binary symmetry axis, so that additional degeneracy arises from this rotational equivalence.

Despite having less stereoisomers (12),[7] as compared with monoradical **2b**, the interconversion graph of chlorocarbon **2a** is, by far, the most difficult to interpret in detail (Figure 7). The only apparently clear feature is, perhaps, the 3-fold degeneracy arising from the rotational symmetry of one of the diastereomeric forms. On the other hand, it is quite striking to note that many of the interconversion processes are direct enantiomerizations. This situation occurs although the structure has six formal stereogenic elements and, given the rearrange-

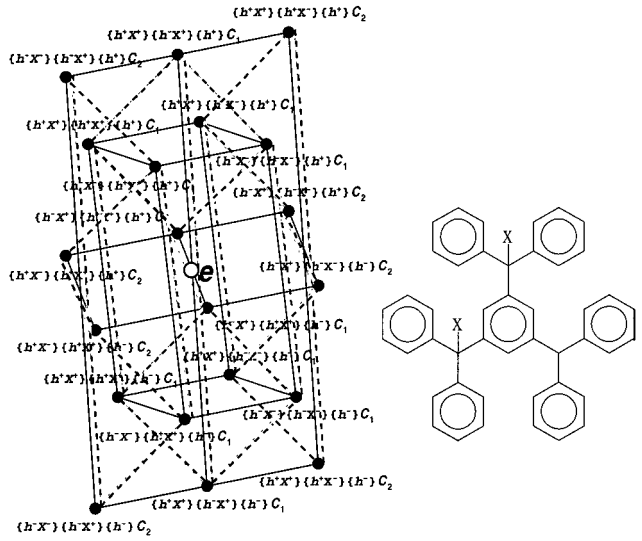

Figure 6. Interconversion graph of molecule **2b**. Short-dashed lines: M_1 pathways. Solid lines: M_2 pathways. An open circle (*e*) denotes an enantiomerization/inversion center.

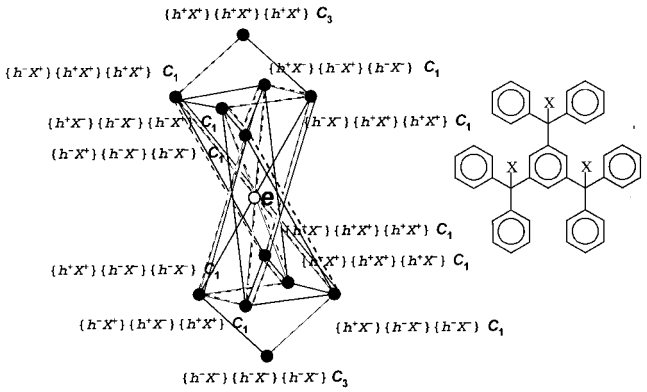

Figure 7. Interconversion graph of molecule **2a**. Short-dashed lines: M_1 pathways. Solid lines: M_2 pathways. An open circle (*e*) denotes an enantiomerization/inversion center.

ment modes described, a maximum of two stereogenic elements change their respective configurations at a time. In our opinion, this brings out, perhaps in the boldest way possible, the complex spatial relationships existing among all three constitutionally equivalent moieties.

Additional Interconversion Graphs. The graphs presented so far, albeit very useful from a theoretical point of view for describing the interconversion pathways of stereoisomers, are not appropriate for dealing with the experimental results presented in the oncoming Sections since all these experiments have been carried out in achiral environments. It is then obvious that a great deal of clarity is gained by simplifying the original graphs, so that they only carry the information relevant to the "experimentally observed" interconversions between diastereomeric forms. For distinction purposes, we will call these new reduced graphs "*diastereomeric interconversion graphs*". In this respect, Figure 8 shows the reduced graphs corresponding to hydrocarbons **1a** and **2a**, as derived from Figures 4 (bottom) and 7, respectively.

A second useful set of graphs are those showing the interconversions of the H atoms of different stereoisomers. These graphs can be directly related to the results of 2D *EX*change *S*pectroscop*Y* (EXSY) NMR experiments performed on the compounds. For this purpose, all

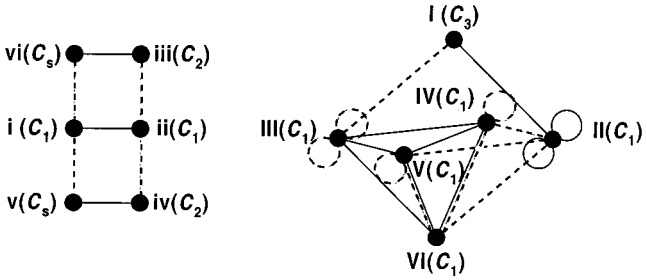

Figure 8. Diastereomeric interconversion graphs for molecules **1a** (left) and **2a** (right). Short-dashed lines denote M_1 pathways, solid lines show M_2 pathways, and loops indicate direct enantiomerization paths. For the sake of clarity, diastereomeric forms have been labeled as shown in Table 3.

diastereotopic, i.e., anisochronous, protons pertaining to the whole set of diastereomeric forms must be differentiated from each other, so that interconversions taking place among them are suitably depicted. The derivation of these graphs, hereafter called "*proton-exchange graphs*", involves the labeling of protons in each diastereomer, since only in this way it is possible to keep track of their changes through the interconversion network. In this respect, it should be taken into account that each triaryl moiety supports only one H atom, which acts as the X (central) substituent of the helix. Therefore, for series **1** and **2**, labeling of moieties is equivalent to labeling of protons. Moreover, since all X-substituents are H nuclei, their orientation and position, *as shown in the symmetry-adapted symbolic notation* used so far, is a straightforward indication of a given, distinct magnetic surrounding. This means that the above-mentioned symbolic notation becomes appropriate, with only minor modifications concerning labeling, for assignment purposes. Conversely, in the context of NMR spectroscopy, changes in chemical shifts of proton signals are the *simplest* probes of the interconversion processes taking place in our systems.

Figure 9 shows the proton-exchange graphs derived for chlorocarbons **1a** and **2a**, the only diamagnetic species belonging to families **1** and **2** and, thus, the only molecules under study for which NMR experiments are feasible.[19,20] For **1a**, the diastereomeric interconversion pattern shown in Figure 8 (left) is easily recognizable in the proton-exchange graph (Figure 9, left), because four diastereoisomers have symmetry-equivalent protons. This situation becomes more complicated by inspection of the proton-exchange graph corresponding to chlorocarbon **2a** (Figure 9, right). The lack of symmetry elements in most diastereomers of **2a** causes a dramatic increase in the number of proton-exchange paths, as compared with the number of interconversion paths among diastereoisomers depicted in Figure 8 (right).

^{1}H NMR Assignments of 1a and 2a Isomer Mixtures. The ^{1}H NMR spectra of **1a** and **2a** show the expected number of resolved signals, taking into account the number of isomers and their symmetry. From the NMR point of view, protons in **1a** and **2a** are isolated from each other, both in terms of scalar couplings and in the possibility of cross-relaxation. This results in very

(19) The dynamic stereochemistry of structurally simple open-shell molecules, such as **1a** and **2a**, has already been studied by techniques such as ESR, HPLC, and Dynamic-HPLC (see ref 20).

(20) Veciana, J.; Crespo, M.-I. *Angew. Chem., Int. Ed. Engl.* **1991**, *30*, 74−76.

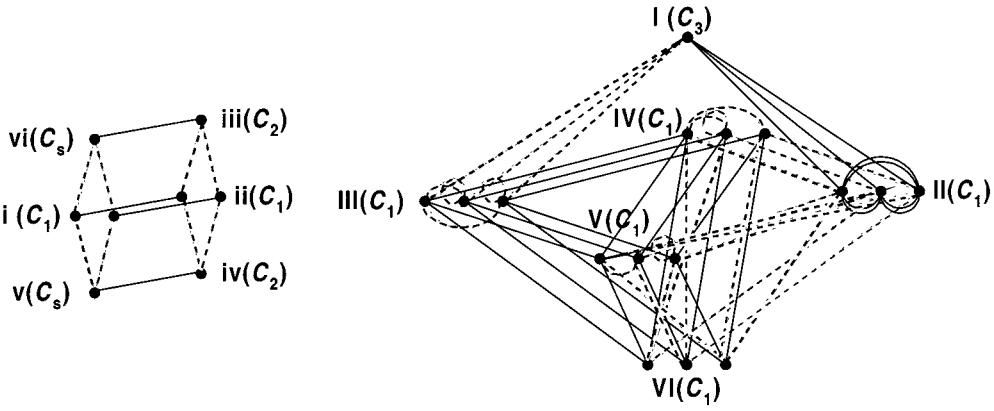

Figure 9. Proton-exchange graphs of molecules **1a** (left) and **2a** (right). Short-dashed lines indicate M_1 pathways, and solid lines denote M_2 pathways. For the sake of clarity, diastereomeric forms have been labeled as shown in Table 3.

Table 3. Labeling of Diastereomeric Forms Corresponding to Molecules 1a and 2a

molecule	diastereomer	symmetry	label
1a	$\{h^+X^+\}\{h^+X^+\}/\{h^-X^-\}\{h^-X^-\}$	(C_1)	i
	$\{h^+X^+\}\{h^-X^-\}/\{h^-X^-\}\{h^+X^+\}$	(C_1)	ii
	$\{h^+X^-\}\{h^+X^+\}/\{h^-X^+\}\{h^-X^-\}$	(C_2)	iii
	$\{h^+X^+\}\{h^+X^-\}/\{h^-X^-\}\{h^-X^+\}$	(C_2)	iv
	$\{h^+X^+\}\{h^-X^+\}$	(C_s)	v
	$\{h^+X^-\}\{h^-X^-\}$	(C_s)	vi
2a	$\{h^+X^+\}\{h^+X^+\}\{h^+X^+\}/\{h^-X^-\}\{h^-X^-\}\{h^-X^-\}$	(C_3)	I
	$\{h^-X^-\}\{h^+X^+\}\{h^+X^+\}/\{h^+X^+\}\{h^-X^-\}\{h^-X^-\}$	(C_1)	II
	$\{h^-X^+\}\{h^+X^+\}\{h^+X^+\}/\{h^+X^-\}\{h^-X^-\}\{h^-X^-\}$	(C_1)	III
	$\{h^-X^+\}\{h^+X^-\}\{h^+X^+\}/\{h^+X^-\}\{h^-X^+\}\{h^-X^-\}$	(C_1)	IV
	$\{h^-X^+\}\{h^+X^+\}\{h^+X^-\}/\{h^+X^-\}\{h^-X^-\}\{h^-X^+\}$	(C_1)	V
	$\{h^+X^-\}\{h^+X^+\}\{h^+X^+\}/\{h^-X^+\}\{h^-X^-\}\{h^-X^-\}$	(C_1)	VI

long relaxation times (T_1 = 7−8 s) and opens the possibility of characterizing relatively slow interconversion pathways using 2D EXSY techniques. However, for the correct interpretation of the results the spectra have to be completely assigned. Hetero multiple bond coupling (HMBC)[21] spectra were used to unambiguously correlate sets of signals arising from the same stereoisomer as described in detail in the preceding paper.[7] Briefly, two protons belonging to propeller units that share an aromatic ring can be related because they show three-bond couplings to the same carbon atom in this common ring. In the case of three-propeller molecules (i.e., **2a**) the three carbons of the central aromatic ring in ortho positions with respect to the proton-bearing substituents can similarly be related as they are pairwise coupled to each proton giving a characteristic pattern that correlates the three protons of each isomer. In the case of **2a**, HMBC spectra directly allow the assignment of the proton signal from isomer I, as it is the only one with C_3 symmetry. For the remaining signals of **1a** and **2a** the assignment of each NMR signal, or set of signals, to a particular isomer has to be addressed. Tables 4 and 5 show the labeling of the different isomers of chlorocarbons **1a** and **2a**, as well as the labeling of the resonance signals and the corresponding chemical shifts.

The large spectral dispersion observed in the proton NMR spectra of **1a** and **2a** arises from the geometric dependency of the aromatic ring currents from all the aromatic rings of each isomer on each proton. Different models have been suggested to calculate ring current shifts.[22] However, the more important concern for non-rigid systems, such as the ones under study, is the presence of fast averaging between different conformations adopted by each isomer. This issue has been approached by averaging the geometric contribution to ring current shifts contributions, calculated using the simplest point dipole approximation for the sake of computational demands, along a 10 ps molecular dynamic

Table 4. Calculated *G*(i) Values and Experimental Chemical Shifts Assignments for the Isomers of 1a

isomer[a]	calcd: $G(i) \times 10^2$ (Å^{-3})		*e*xptl: δ_{exp}[b,c] (ppm)	
i	6.35	6.95	6.72 (A)	6.93 (F)
ii	6.78	6.64	6.90 (E)	6.89 (D)
iii	6.64		6.84 (C)	
iv	6.99		6.94 (G)	
v	6.60		6.78 (B)	
vi	6.89		6.95 (H)	

[a] Isomer labeling is defined in Table 3. [b] In $CDCl_3$ at 298 K. [c] Signals are labeled by capital letters in order of increasing frequency.

Table 5. Calculated *G*(i) Values and Experimental Chemical Shift Assignments for the Isomers of 2a

isomer[a]	calcd: $G(i) \times 10^2$ (Å^{-3})			exptl: δ_{exp}[b,c] (ppm)		
I	6.45			6.72 (E)		
II	6.56	6.32	6.74	6.83 (I)	6.68 (B)	6.93 (N)
III	6.09	6.98	6.63	6.60 (A)	7.00 (P)	6.80 (H)
IV	6.82	6.73	6.95	6.92 (M)	6.89 (L)	6.98 (O)
V	6.43	6.58	6.37	6.74 (F)	6.78 (G)	6.71 (C)
VI	6.38	6.72	6.70	6.72 (D)	6.84 (K)	6.83 (J)

[a] Isomer labeling is defined in Table 3. [b] In $CDCl_3$ at 298 K. [c] Signals are labeled by capital letters in order of increasing frequency.

(21) Bax, A.; Summers, M. F. *J. Am. Chem. Soc.* **1986**, *108*, 2093−2094.

(22) Johnson, C. E.; Bovey, F. A. *J. Chem. Phys.* **1958**, *29*, 1012−1014. Haigh, C. W.; Mallion, R. B. *Org. Magn. Reson.* **1972**, *4*, 203−228. Abraham, R. J.; Fell, S. C. M.; Smith, K. M. *Org. Magn. Reson.* **1977**, *9*, 367−373.

simulation at 300 K starting from an energy minimized conformation representative of each isomer. Under these conditions no transitions between isomers are observed. Thus, for each proton *i*, we calculated a mean geometrical parameter *G*(i) according to eq 1

$$G(\mathrm{i}) = \left\langle \sum_{j=1,n} \left(\frac{1 - 3\cos^2\theta_{ij}}{r_{ij}^{\,3}} \right) \right\rangle \qquad (1)$$

where r_{ij} is the distance of that proton to the center of each of the *n* aromatic rings of the molecule ($n = 5$ for **1a** and $n = 7$ for **2a**) and θ_{ij} is the angle between the line joining the observed proton to the center of ring j and the normal to the average plane of the ring. The angular brackets denote an average over the molecular dynamics trajectory. Calculated *G*(i) values and experimental chemical shifts, $\delta_{\mathrm{exp(i)}}$, of the isomers of **1a** and **2a** are given in Tables 4 and 5, respectively.

Experimental chemical shifts are the sum of the contribution from ring current shifts and a geometrically independent component δ_0 that takes into account all other kinds of contributions and which we assume constant for the different isomers of each molecule:

$$\delta_{\mathrm{exp}}(\mathrm{i}) = KG(\mathrm{i}) + \delta_0 \qquad (2)$$

Thus, for the correct assignment, a plot of $\delta_{\mathrm{exp(i)}}$ versus *G*(i) should be linear. In addition, although individual chemical shifts are subject to considerable experimental variations and the method used for the calculations is by no means rigorous, the HMBC derived correlations of protons belonging to the same isomer allow us to compare differences in *G*(i) values and experimental shifts between protons belonging to the same species. These values are expected to be less sensitive to environmental effects than the absolute chemical shifts of different isomers and allow a preliminary assignment using only semiquantitative arguments.

For the isomers of **2a**, the *G*(i) differences for the three protons of the isomer III only match those found in the set of resonances A, H, and P. The isomer predicted to have its three protons resonating at higher frequency is the isomer IV and, therefore, is assigned to the L, M, and O set of signals. Analogously, the set of C, F, and G signals is assigned to isomer V predicted to give the three resonance signals at the lowest frequency. The pattern of D, J, and K resonances with two nearly degenerate signals at lower field of the third one matches the predicted one for isomer VI. The remaining isomer II is finally assigned to resonances labeled as B, I, and N.

Figure 10 shows a plot of δ_{exp} versus *G*(i) for protons in the isomers of **2a** using the assignment given in Table 5. The straight line is the best fit to eq 2 and has a regression coefficient of 0.96. The values of *K* and δ_0 can be calibrated from this fit. Alternative assignments give rise to lower linear regression coefficients (see the Supporting Information). In the case of the chlorocarbon **1a**, the presence of several isomers with C_2 or C_s symmetries that give rise to a single proton signal, and the small chemical shift differences between some of the isomers makes the assignment, based solely on chemical shift considerations, not unique. The assignment shown in Table 4 provides a regression coefficient of 0.88 between δ_{exp} and *G*(i). A cyclic permutation of the assignments of protons F, G, and H would give a slightly better coefficient of 0.90 but this assignment is incompatible with HMBC spectra showing that protons F and A belong to the same C_1 symmetry isomer. Interchanging of the assignments of nearly degenerate protons G and H would also not significantly modify the regression coefficient. However, this alternative assignment can also be rejected, as it would be incompatible with the exchange patterns derived from EXSY experiments (see below).

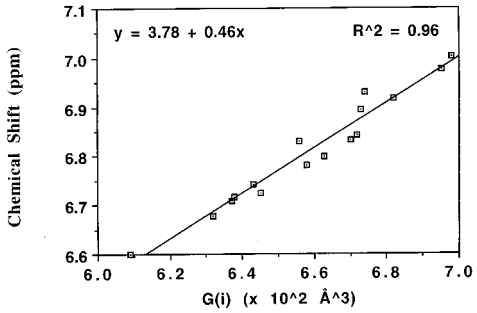

Figure 10. Plot of chemical shifts δ_{exp} versus *G*(i) values for chlorocarbon **2a** at 298 K.

Experimental Exchange Patterns. The presence of bulky chlorine substituents in compounds **1a** and **2a** reduces the rate of exchange between isomers and allows the observation of separate signals from the different species present in solution. On the other hand, the isolation of the protons results in the absence of efficient relaxation pathways and causes very long relaxation times. Therefore, unusually long mixing times can be used in EXSY spectra and most of the rearrangement processes can be demonstrated by the presence of cross-peaks relating pairs of proton signals whose environments are exchanged by isomerization processes. Thus, EXSY spectra provide direct evidence for the rearrangement processes predicted in the first part of this paper. Rate constants for the observed interconversions can be obtained from integration of EXSY spectra as described by Abel et al.[23]

(a) Isomeric Interconversion of Two-Propeller Compound 1a. Figure 11 shows a plot of an 2D-EXSY spectrum of **1a** at 298 K using a mixing time of 8 s. The exchange pattern derived from EXSY experiments is presented graphically in Figure 12. By comparing Figure 12 with the theoretical proton-exchange graph presented in Figure 9, it is clear that the experimental graph is a subgraph of the theoretical one. Thus, of the topologically possible pathways, those linking isomers ii and iii and i and v are not observed experimentally while the remaining five give rise to cross-peaks. On the other hand, all the observed exchange processes have to correspond to topologically allowed possibilities. Thus, any remaining ambiguities in the assignment of the signals from different protons initially made from chemical shift considerations could be solved at this point.

Figure 13 shows the only four possible assignments (A1−A4) of protons to the distinct isomers of **1a** that would be compatible with the experimentally observed exchange processes. Using only the information from HMBC spectra would provide 48 possible assignments. The four assignments arise from the two possible locations for C_1 and C_2 isomers and the fact that once the locations of C_1 and C_2 isomers have been chosen, those

(23) Abel, E. W.; Coston, T. P. J.; Orrell, K. G.; Sik, V.; Stephenson, D. *J. Magn. Reson.* **1986**, *70*, 34−53.

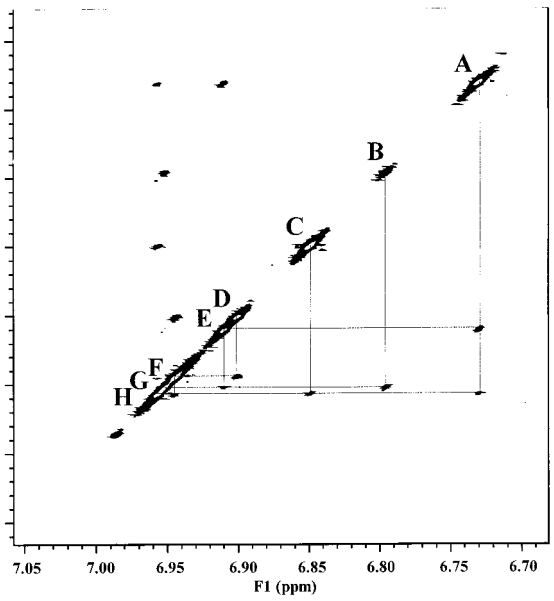

Figure 11. 2D-EXSY-NMR spectrum of chlorocarbon **1a** at 298 K (mixing time: 8 s). Proton sites are labeled in order of increasing frequency along the diagonal.

of both C_s isomers are fixed and noninterchangeable. The linear regression coefficient for the correlation between δ_{exp} and G(i) using these four assignments are 0.88 (A1), 0.05 (A2), 0.23 (A3), and 0.07 (A4), respectively. Thus, the combined use of chemical shift arguments and the observed exchange patterns provides an unequivocal assignment of the ^{1}H NMR spectrum of the mixture of isomers of **1a**.

Table 6 gives the measured rates of exchange between isomers of **1a** at 298 K along with their populations. Forward and reverse rate constants are not the same, and their ratio equals the equilibrium constant for the interconversion of each pair of isomers. The measured rates for the observed interconversions show a rather narrow distribution. Nonobserved exchange pathways have rate constants smaller than 10^{-4} s^{-1}. The higher energy less populated isomers iv and v tend to give higher interconversion rates, suggesting that the energy differences between isomers in the ground state are larger than the differences between transition states.

The three predicted M_2 modes are observed experimentally while only two of the four topologically allowed M_1 modes have activation energies low enough to allow their observation. Comparing isomerization pathways belonging to the two modes and departing from the same isomer, in three of the four cases (i.e., vi ← i → ii, i ← ii → iv, ii ← iv → v) the M_2 mode rearrangements are from 40% to 160% faster than the ones belonging to a M_1 mode. In the remaining example (iii ← vi → i) the M_1 mode is about 30% faster.

(b) Isomeric Interconversion of Three-Propeller Compound 2a. Figure 14 shows a plot of an EXSY spectrum from the **2a** isomer mixture, and the exchange processes deduced from it are presented in Figure 12. Exchange rates are given in Table 7.

In contrast to the case of the two-propeller compound **1a**, for **2a** several enantiomerization processes are expected to be detectable by NMR as they lead to exchange between protons belonging to the same isomer. Isomer II is the only one that is predicted to have an enantiomerization pattern causing the mutual exchange of all three proton signals. The experimental observation of mutual exchange between the three protons I, B, and N but not for any other complete set of protons in the other isomers confirms the assignment deduced from chemical shift arguments. Additional enantiomerization processes, leading to the exchange of only two protons of the same isomers, were observed for isomers IV (protons L and O) and III (protons H and A). Both were predicted to be topologically allowed using the analysis presented in the first part of the paper. The enantiomerization processes leading to the exchange of protons H and P in isomer III and C and F in isomer V, although topologically allowed, were not detected even at 318 K.

Of the topologically allowed interconversions between different isomers, those between isomers I and III, VI and II, and II and V were not detected experimentally even at 318 K in $CDCl_3$. All of them belong to the M_1 type. Interconversion between IV and VI could proceed either by an M_1 or an M_2 pathway. Each type would give rise to a different exchange pattern of protons in the two species and, therefore, is distinguishable experimentally. Again, only the M_2 rearrangement is observed in this case. Thus, while all eight M_2-type rearrangements give rise to detectable cross-peaks, only three out of eight M_1 pathways have activation energies low enough to be detected in our experiments. Of these, two are the enantiomerizations of isomers III and IV. However, the observed M_1 rearrangements include some of the fastest rates measured in this system (e.g., the enantiomerization of IV and III), and the M_1 isomerization from II to IV is eight times faster than the M_2 rearrangement of the same isomer leading to I. As observed for **1a**, the highest energy isomer (IV) in general shows the fastest interconversion processes (except for IV → VI) and the most populated isomer (VI) has the lowest rearrangement rates. This observation suggests that for the three propeller molecules the energy differences between isomers are also lower than between the transition states interconverting them.

This trend is not followed by the isomer I, with C_3 symmetry. In this case, the rate of isomerization to II is lower than expected on the basis of its population. This result is not unexpected considering the loss of symmetry between the starting species and the transition state that does not occur in any of the other rearrangements between isomers of **2a**.

NMR experiments only allow the differentiation of two modes of rearrangement, M_1 and M_2. Each of these modes of rearrangement could be the result of several interconversion mechanisms involving the flip of different aromatic rings. For **1a** and **2a**, the presence of bulky chlorine substituents in the ortho positions of the aromatic rings would result in very high activation energies for zero or one-ring flips in individual propellers. On the other hand, two-ring flips have been found to be the threshold mechanism for many systems. Assuming also this mechanism for our systems, an M_1 mode of rearrangement implies the flip of the two outer rings. Similarly, an M_2 mode of rearrangement corresponds to a flip of an outer and an inner aromatic ring although a three-ring flip involving the flip of the inner and the two outer rings would also be compatible with the observed exchange. Thus, whatever is the microscopic mechanism, an M_2 rearrangement implies the flip of the inner ring, common to the different propellers.

Table 6. Rate Constants, k_{ij},[a] for Conformational Interconversions between Isomers of 1a at 298 K

	$k_{ij} \times 10^3$ (s)					
	iii	vi	i	ii	iv	v
iii		2.3 ± 0.4				
vi	3.3 ± 0.6		4.2 ± 0.4			
i		1.8 ± 0.2		3.8 ± 0.2		
ii			5.9 ± 0.4		2.2 ± 0.4	
iv				5.3 ± 0.5		7.5 ± 0.7
v					16.5 ± 1.5	
populations	19.4	13.8	32.4	20.8	9.3	4.2

[a] Average of two determinations using mixing times of 8 and 10 s.

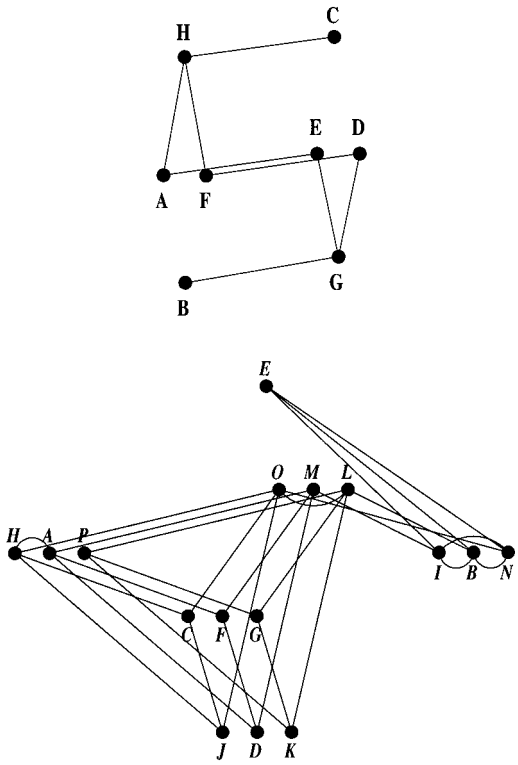

Figure 12. Experimental proton-exchange graphs for chlorocarbons **1a** (top) and **2a** (bottom).

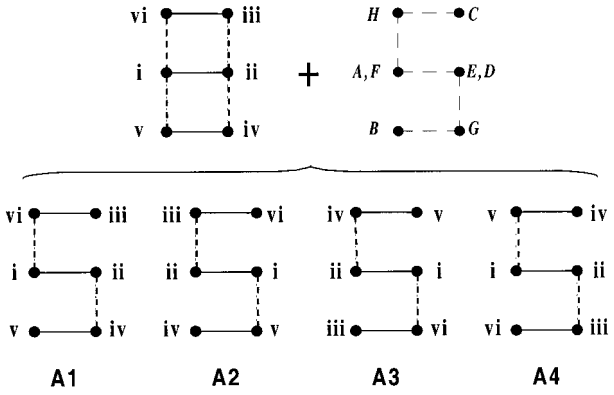

Figure 13. Compatible assignments (A1−A4) of each of the eight H atom signals (A, B, ..., G) to the six different stereoisomers (i, ii, ..., vi) arising from the combination of theoretical and experimental diastereomeric reduced graphs for chlorocarbon **1a**.

The experimentally observed preference for M_2 mode rearrangements is higher for the three-propeller molecule **2a** than for the two-propeller **1a**. This fact could be related to the larger steric hindrance of the former that reduces the energy barrier for the flip of the inner ring

Summary

For the first time, the static and the dynamic stereochemistry of molecular two- and three-propellers have been analyzed in detail. The theoretical analysis outlined so far has allowed us to discuss the dynamic stereochemistry of seven multipropeller structures in a unified way, regardless of their stereochemical complexity, which has been shown to be of a remarkable variety. From a theoretical point of view, our starting point has been the classification of interconversion mechanisms established for simple molecular propellers by Mislow and co-workers.[1,2] We have shown that these mechanisms can be translated straightforwardly to our systems and thoroughly analyzed using a procedure that employs a symbolic notation and set of simple, binary transformation rules.

Although each propeller has only two experimentally distinguishable rearrangement modes, the existence of multiple propeller-like moieties gives rise to complex interconversion patterns. To visualize these patterns in a proper fashion, suitable interconversion graphs were provided for all species under study.

2D-EXSY experiments were performed for diamagnetic two- and three-propeller molecules **1a** and **2a**, which are the most complex of each series. Complete assignments of the ^{1}H NMR spectra could be performed and the observed pathways were found to be a subset of the topologically allowed ones. For both molecules, but especially for the three-propeller **2a**, M_2 pathways, involving the flip of the inner aromatic ring, seem to be observed preferentially although not exclusively. A quantitative analysis of the measurable rates suggests that the energy differences between isomers are larger than between the low energy transition states for their interconversion.

Experimental Part

Compounds **1a** and **2a** were prepared and purified as described elsewhere.[4,5] NMR spectra were obtained at 500 MHz spectrometers using 4096 × 512 data points that were zero-filled in F2 and extended by linear prediction in F1 to give an 8192 × 2048 matrix. The solvent used for the spectra was $CDCl_3$. Spectral widths were 820 Hz (^{1}H) and 2515.4 Hz (^{13}C) for **2a** and 169.8 (^{1}H) and 2515.4 Hz (^{13}C) for **1a**. The total recycle time was 9 s (**2a**) or 10 s (**1a**). EXSY spectra were obtained in a 500 MHz instrument. For **2a** a spectral width of 516.9 Hz and an acquisition time of 3.96 s was used. Data were acquired using 4096 × 512 points and processed using 4096 × 1024 complex points. Gaussian apodization was only used in the F1 dimension. Spectra were recorded at 298 K using

Table 7. Rate Constants, k_{ij},[a] for Conformational Interconversions between Isomers of 2a at 298 K in $CDCl_3$

	$k_{ij} \times 10^3$ (s)					
	I	II	IV	V	VI	III
I		0.9 ± 0.7				
II	0.8 ± 0.6	3.9 ± 0.8	6.5 ± 1.0			
IV		16 ± 4.4	8.4 ± 2.6	7.8 ± 1.8	0.6 ± 0.5	8.1 ± 0.8
V			6.7 ± 2.5		1.3 ± 0.7	3.1 ± 0.4
VI			0.2 ± 0.2	0.6 ± 0.3		0.6 ± 0.2
III			6.6 ± 0.6	3.7 ± 0.5	2.0 ± 0.9	12.0 ± 4.1
populations	16.0	20.2	9.4	14.3	27.9	12.1

[a] Average of three experiments with mixing times of 6, 8, and 10 s.

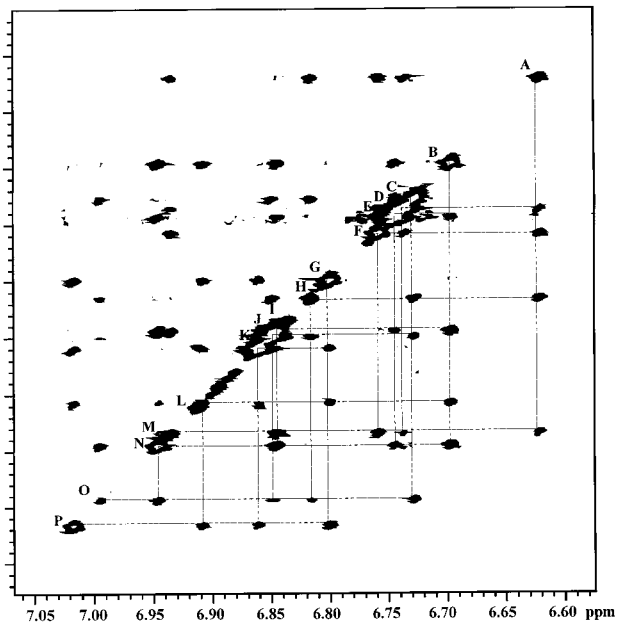

Figure 14. 2D-EXSY-NMR spectrum of chlorocarbon **2a** at 318 K (mixing time: 8 s). Proton sites are labeled in order of increasing frequency along the diagonal. At this temperature, sites I and J are resolved allowing the assignment of the respective exchange cross-peaks.

mixing times of 4, 6, and 8 s with a recycle time of 12 s and a mixing time of 10 s with a recycle time of 14 s. EXSY spectra were also recorded with a mixing time of 6 s at temperatures of 303, 308, 313 and 318 K. EXSY spectra of **1a** were recorded at 298 K using an spectral width of 352.3 Hz, an acquisition time of 2.907 s and a mixing time of 8 s (recycle time 11 s) or 10 s (recycle time 13.4 s). Additional spectra were recorded at 303 K and with a mixing time of 8 s. After transformation, the spectra were baseline corrected in both dimensions and integrated using the proper software. Populations were extracted from the integration of 1D NMR spectra of the same samples. The errors were estimated by comparing the rate constants measured for individual proton-exchange processes in two or three independent experiments.

The geometrical factor for the point dipole estimation of the aromatic contribution to chemical shifts was calculated as follows. Starting conformations were generated and minimized using an empirical force field (Insight II software). Molecular dynamic simulations were carried out in a vacuum using the CVFF force field of *Discover*, for 10 ps with a time step of 1 fs, and structures were stored every 10 fs. For each structure, the average plane and center of each aromatic ring was calculated and from these the distance and θ angles to each proton. For each proton, the contribution from all the aromatic rings in the molecule were added and the result was averaged along the trajectory. Plotting selected dihedral angles along the trajectory monitored the absence of conformational transitions to other isomers.

Acknowledgment. This work was supported by grants from DGES (PB96-0862-C02-01 and PB97-0933), CIRIT (1998SGR-0106 and 1997SGR-102), and the 3MD Network of the TMR program of the E.U. (ERBFMRXCT 980181). We thank Dr. D. B. Amabilino (ICMAB, CSIC) for correcting the manuscript and also for his useful comments and suggestions. J.S. and N.V. also thank the MEC for fellowships.

Supporting Information Available: Calculated and experimental chemical shifts for EXSY compatible assignments for chlorocarbons **1a** and **2a** (Tables S1 and S2**)**. Compatible assignments (A1−A8) of 16 hydrogen signals (A, B, ..., P) to the six stereoisomers (I, II, ..., VI) for chlorocarbon **2a** (Figure S1). This material is available free of charge via the Internet at http://pubs.acs.org.

JO000474G